




Generic accommodations of an atom in the Lennard-Jones fcc and hcp rare-gas solids: A computational study

Georgiy K. Ozerov ^{1,*}, Dmitry S. Bezrukov ^{1,2} and Alexei A. Buchachenko ¹

¹*Skolkovo Institute of Science and Technology, Skolkovo Innovation Center, Nobel str. 3, Moscow 143026, Russia*

²*Department of Chemistry, M.V. Lomonosov Moscow State University, Moscow 119991, Russia*



(Received 3 January 2021; revised 16 March 2021; accepted 25 March 2021; published 26 May 2021)

A comprehensive computational analysis of the stable accommodations of an atom in the Lennard-Jones (LJ) face-centered-cubic (fcc) and hexagonal-closest-packed (hcp) lattices is presented. For a wide range of the guest-host LJ interaction parameters and the number of host atoms removed, N , global optimizations are performed to find the minimum energy structures. Stable accommodations are determined using the convex hull of the energy dependence on N . The most stable ground accommodations are mapped onto the guest-host LJ parameter space for the hosts representing the rare-gas solids from Ne to Xe. The radial distribution function analysis is used to classify the structures found as originating from the guest placements in the lattice voids or at the node. Ten generic accommodations are identified for each lattice. Comparing to mostly polyhedral structures in fcc, the hcp ones have generally lower symmetry, which should affect the band shapes of atomic absorption spectra. Despite the well-known wrong prediction of higher hcp phase stability in the LJ model, the cases of strong accommodation preferences in one phase or another are identified. Being generic, the obtained results can be useful for a qualitative interpretation of atomic matrix isolation experiments.

DOI: [10.1103/PhysRevB.103.184110](https://doi.org/10.1103/PhysRevB.103.184110)

I. INTRODUCTION

Cryogenic rare-gas (RG) solids provide a very convenient inert environment for isolating and detecting metastable and highly reactive chemical species. The soft and (generally) nonmagnetic nature of these compressible solids and their transparency in a wide spectral range make it possible to deposit or generate various atomic and molecular species and characterize them using a variety of spectroscopic techniques, laying the foundation of matrix isolation spectroscopy; see, e.g., Refs. [1–5]. In comparison to this mainstream topic, less attention has been paid to the fact that the spectra of isolated species yield important information on the structure of the host solid. This is especially true for atomic and nonpolar molecular guests, whose interaction with the host has the same weak dispersion nature as the interaction that holds the host solid together. Most of the related studies concentrate on the point defects, or more precisely, on how the matrix accommodates the impurities. The electron paramagnetic resonance, infrared and optical spectroscopy, recombination-induced thermoluminescence, neutron scattering, and x-ray absorption spectroscopy have been proven to be useful in revealing the nature, symmetry, and sometimes the structure of the stable atomic and molecular trapping sites in RG solids (see Refs. [6–14] for selected examples).

Moreover, it is also known that matrix isolation studies can probe and affect the phase composition and disorder of the host. A particularly interesting issue is the existence of the two solid RG phases, namely the face-centered-cubic (fcc)

and hexagonal-closest-packed (hcp) ones [15]. The hexagonal phase appears mostly in the nonequilibrium conditions [16–19], indicating that the stable one has fcc packing. Modeling of the crystal structure using the Lennard-Jones (LJ) atom-atom potentials inevitably gives a slight preference to the hcp phase [20–22], and the same is apparently true for more realistic pairwise potentials [23]. Numerous explanations of the controversy using surface effects, distinct equilibration pathways, many-body interactions, and phonon contributions were considered; see, for instance, Refs. [24–26]. The most accurate analysis to date [27] points to the phonon coupling as the decisive factor stabilizing the fcc phase. Still, the mechanism of the fcc to hcp phase transition is not well understood despite numerous experimental and theoretical studies (see Refs. [26,28–31] and literature cited therein).

Being sensitive to the surrounding, the spectroscopy of impurities may serve as a probe for the phase composition of the matrix. The most certain example is the hindered rotation of methane and some other spherical-top molecules. The structure of infrared absorption spectra [8,32] and neutron scattering patterns [11,33–35] revealed rotational transitions firmly assigned to distinct guest accommodations in the pure fcc and hcp crystallites and at the stacking faults of the hcp phase. The coexistence of the two phases and the stacking faults was also suggested to interpret the electron spin resonance (ESR) spectra of a hydrogen atom and methyl radical [6,36], the absorption spectra of a barium atom [37–39], and the excitation and fluorescence spectra of some diatomic molecules [40–42]. The interesting observation that impurities can induce the local fcc to hcp phase transition was reported by Savchenko and co-workers [43], who monitored the

*Corresponding author: g.ozarov@skoltech.ru

luminescence of Ar, Kr, and Xe atoms in the Ne matrix excited by electron-impact excitation. The formation of quite extended hcp domains was found at impurity concentrations as low as 0.01%.

Although these observations strongly suggest the possibility of spectral monitoring of the metastable phase formation in RG solids, no systematic modeling of the stable accommodations of impurities in an hcp lattice and their comparison with those inherent to fcc has been performed (except for one that was exemplary for the large planar anthracene molecule [44]). Understanding the generic structure of the stable trapping sites pertinent to two crystal phases should reveal the differences in the respective spectral signatures, while a comparison of their relative energies should provide insight into the preferential occupations and the propensity to local phase transitions.

In this paper, we present a comprehensive computational analysis of atomic accommodations in the fcc and hcp RG lattices. We employed the pairwise LJ model, a conventional zero-order approximation to RG-RG interactions that can uncover generic results and general guidelines. In addition, the LJ model is universal, thus it can scale to any host parameters. Unbiased global structure optimization in the wide physically meaningful ranges of interaction parameters followed by thermodynamic stability assessment provided exhaustive lists of generic accommodations in each lattice, classified by effective size, structure type, and symmetry. The difference between the ground accommodation energies in two lattices was analyzed, and the cases of strong preference were found at an energy scale much larger than the deficiency of the LJ model for the pure phases.

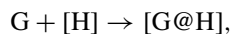
II. COMPUTATIONAL

The techniques used for structure generation, thermodynamic stability assessment, and symmetry classifications have already been tested for stable accommodations of atoms and dimers in the LJ fcc Ar lattice [45,46]. This work extends the fcc results to wider parameter ranges, other hosts (Ne, Kr, and Xe), and it covers generic accommodations in the hcp lattice.

A. Crystal trapping site model

The present model for identification of the stable atomic and molecular accommodations in RG crystals was proposed in Refs. [47,48] and further adapted to global searches in Refs. [45,46].

Our aim is to model the equilibrium accommodation process of an atom within the bulk crystal,



where the short-hand notations H and G for the Host RG and the Guest atoms, respectively, are introduced, and square brackets indicate the crystal phase. We assume that the crystal fragment [H] is large enough that we can neglect the surface effects and disregard the defect formation. To distinguish between accommodations that differ in size, we introduce parameter N , the number of host atoms dislodged by the guest from its surrounding in the bulk to the periphery of the crystal,

symbolically,



where M is the total number of host atoms included in the atomic model. The respective accommodation energy, as a function of N , is defined as

$$\Delta E(M, N) = E_{[G@H]}(M, N) - E_{[H]}(M) - E_G - NE^{\text{at}}. \quad (1)$$

The last term here approximates the energy of crystal expansion in terms of individual atomic contributions equal to crystal atomization energy per atom E^{at} . As the overall number of particles in the system is always fixed at $(M + 1)$, the minimum of Eq. (1) in N , N_0 , identifies the most stable (ground) accommodation.

Setting up the numerical procedure, we first consider a large fragment of an ideal host crystal $[H]_M^{\text{fcc,hcp}}$ confined by a sphere centered on an arbitrary H atom. Within this fragment, the lattice constants are optimized by minimizing its energy to $E_{[H]}(M)$ for a given pairwise potential field $u^{\text{HH}}(r_{ij})$, where r_{ij} is the distance between the i th and j th host atoms. To describe the fcc lattice, the single constant $a = a_{\text{fcc}}$ is used. The hcp lattice is generally described by two constants, a_{hcp} and c_{hcp} , which define the base and the height of the hexagonal unit cell, respectively. For the ideal case, they are related to each other as $c_{\text{hcp}} = \sqrt{8/3}a_{\text{hcp}}$ and to an fcc constant as $a_{\text{hcp}} = a/\sqrt{2}$ and $c_{\text{hcp}} = 2a/\sqrt{3}$. Thus, the single constant a is used here to parametrize both lattices. For each lattice, accurate E^{at} values were obtained in the converged calculations with $M \rightarrow \infty$.

At the next stage, we introduce the single guest atom G, which interacts with host atoms by the potential $u^{\text{GH}}(r)$. To this end, the fragment $[H]_M$ is stratified by making a distinction between fixed and movable host atoms. The fixed atoms located far from the center always keep their lattice positions, while the movable ones residing in the central region can be removed, added, and displaced at will upon the sampling, and they should follow the force field upon optimization; see Sec. II C for more details. Replacing N host atoms by G, as described below for the sampling procedure, we minimize the potential energy U to evaluate the term $E_{[G@H]}(M, N)$ in Eq. (1). It should be pointed out here that the dependence on M only reflects the range of u^{GH} interaction and should vanish if M is large enough. From a numerical standpoint, it is a matter of convergence and can be omitted together with the constant term E_G . The simplified expression for the accommodation energy reads

$$\Delta E(N) = E_{[G@H]}(N) - E_{[H]} - NE^{\text{at}}. \quad (2)$$

An analysis of thermodynamic stability entails calculations of the free energy, i.e., an evaluation of the zero-point energy, temperature-dependent phonon contributions, and the work against the pressure. Estimation of these mass-dependent terms would require us to set the atomic masses as the additional model parameters. Moreover, in the low-temperature limit the missed contributions are smaller than the errors in the potential due to the LJ approximation to two-body terms and the omission of higher-order terms in the many-body expansion [23,25,27]. Thus, Eq. (2) is enough to identify the site stability within the NVT or NPT ensemble at the generic coarse energy scale.

In addition to identification of the lowest-energy (ground) accommodation N_0 , Eq. (2) provides a way to find out all the thermodynamically stable trapping sites using the convex hull concept of the discrete composition phase diagrams [49,50]. Indeed, the $\Delta\tilde{E}(N) = \Delta E(N) + NE^{\text{at}}$ quantity gives the accommodation energy for a certain replica of the μVT thermodynamic ensemble. Allowing the exchange of H atoms between replicas in the trapping site disproportionation processes in the spirit of Frost diagrams [51], one can attribute the $\Delta\tilde{E}$ energies forming the convex hull in N to thermodynamically stable trapping sites. As the convex hull condition for a function does not change if a constant or linear correction is added, Eq. (2) is equally applicable for this purpose. In what follows, we mainly consider the ground trapping sites. Higher-lying stable sites with $N \neq N_0$ are discussed only sketchily if they reveal new structure types. We also note that within this approach, only N , an integer measure of the effective trapping site size, is uniquely defined. The features of the corresponding geometric structures should still be deciphered by analyzing the respective atomic configurations.

Accommodation energies for fcc and hcp lattices can be directly compared with each other, with reference to the limits of the respective infinite ideal crystals. The negative or positive difference between the lowest fcc and hcp accommodation energies thus defines the preferred host phase for trapping an atomic impurity with a certain interaction potential with the host.

B. Interaction potentials

For any system $[G@H] \equiv [G@H]_{M-N}$, the total interaction potential is given by

$$U_{[G@H]}(\mathbf{x}) = \sum_{i=1}^{M-N} \sum_{i < j}^{M-N} u_{\text{HH}}(r_{ij}) + \sum_{i=1}^{M-N} u_{\text{GH}}(r_i), \quad (3)$$

where $r_{ij} = |\mathbf{x}_i - \mathbf{x}_j|$ and $r_i = |\mathbf{x}_G - \mathbf{x}_i|$ are the interatomic distances defined through the position vectors of host and guest atoms, \mathbf{x}_i and \mathbf{x}_G , respectively. Each pairwise term has the LJ form

$$u_{\text{HH}}(r) = \epsilon_{\text{HH}} \left[\left(\frac{\rho_{\text{HH}}}{r} \right)^{12} - 2 \left(\frac{\rho_{\text{HH}}}{r} \right)^6 \right]$$

and a similar expression with ρ, ϵ parameters for the $u_{\text{GH}}(r)$ potential.

Our goal is to find generic stable accommodations for an arbitrary guest atom [Eq. (3) only requires an isotropic GH interaction, or zero orbital electronic angular momentum of the guest]. This can be achieved by fixing the host parameters $\rho_{\text{HH}}, \epsilon_{\text{HH}}$ and mapping the stability region of N onto the guest-host interaction parameter plane (ρ, ϵ) [45,46]. The advantage of the LJ potential model is its universality, or the scaling property upon the parameter transformation, e.g., for $(\rho_{\text{HH}}, \epsilon_{\text{HH}}) \mapsto (\rho_{\text{HH}}^*, \epsilon_{\text{HH}}^*)$,

$$u_{\text{HH}}^*(r) = \frac{\epsilon_{\text{HH}}^*}{\epsilon_{\text{HH}}} u_{\text{HH}} \left(\frac{\rho_{\text{HH}}}{\rho_{\text{HH}}^*} r \right).$$

The same scaling obviously applies to the total potential U (3), so the stability analysis can be performed once the $(\rho_{\text{HH}}, \epsilon_{\text{HH}})$ parameters are fixed, and then it can be extended to other host

potentials (provided that the coverage of the ρ, ϵ parameter plane is good enough).

C. Sampling and optimization

Once the reference host parameters $\epsilon_{\text{HH}}, \rho_{\text{HH}}$ are fixed, the global minimum (3) should be found in the configuration space within the nested loops over ϵ, ρ , and N values. To perform the numerous global searches efficiently, we followed the strategy described in Ref. [46].

In brief, further subdivision of the movable atom region was introduced to minimize the efforts to find identical configurations. Atomic embedding and removal at the sampling stage were restricted to the very central “active” region with a radius of about $2a$. Combinatorial presampling within the central region used the auxiliary lattice of vacant positions that included all nodes, natural lattice voids, and face and edge centers. All the combinations of the node occupations (host atom, guest atom, no atom) that comply with certain N were probed, and 6–12 configurations with the lowest energies were selected. After checking and tuning the stratification to preselected energy cutoffs, the global optimization based on the Metropolis algorithm [52–54] with stepwise gradient refinement was performed for each structure, as described in Ref. [46]. At this stage, more layers of host atoms outside the central region were engaged sequentially. The final lowest energy configuration reached in all runs was treated as the global minimum and was refined by the local steepest-descent minimization involving the positions of all movable atoms subjected to small random displacements. This seemingly redundant strategy is a prerequisite for not missing even completely counterintuitive accommodations if they appeared to be a global configuration-space minimum. To avoid any bias, no information on the structures found with other (ρ, ϵ) parameters was used.

As a reference, the Ar host with the parameters $\rho_{\text{HH}} = 3.35 \text{ \AA}$ and $\epsilon_{\text{HH}} = 100 \text{ cm}^{-1}$ was adopted [55]. The initial lattices were generated using 12 translations in each direction of the unit cell with further isolation of the maximum spherical fragment. Next, the central active region with a radius $2a$ was constructed. For each point of the combinatorial presampling, the size of the spherical fragment was checked against the criterion $\max_{i \in \text{surface}} |u_{\text{GH}}(r_i)| / \max_{i \in \text{active}} |u_{\text{GH}}(r_i)| \leq 10^{-6}$. Otherwise, the fragment was enlarged and the procedure was repeated. Typically, the radius of the whole spherical fragment varied from 6 to $9a$. The inner region consisting of movable host atoms was 3– $4a$ on average, depending on the scaling for each initial configuration. The scaling required that the maximum interaction between the G atom and the fixed host atoms be smaller by eight orders of magnitude than the minimum GH interactions for host atoms included in the active region. For the representative case when the GH interaction is equal to the HH one, we considered $M \approx 3600$ host atoms, from which about 3000 atoms were movable (with ~ 150 included in the active region and ~ 450 involved in the global optimization).

As a result, the errors in accommodation energies due to the finite size of the system and energy convergence amounted typically to a few tens of wave numbers. This accuracy is enough to discern the thermodynamically stable sites through the convex hull analysis, except in the border cases.

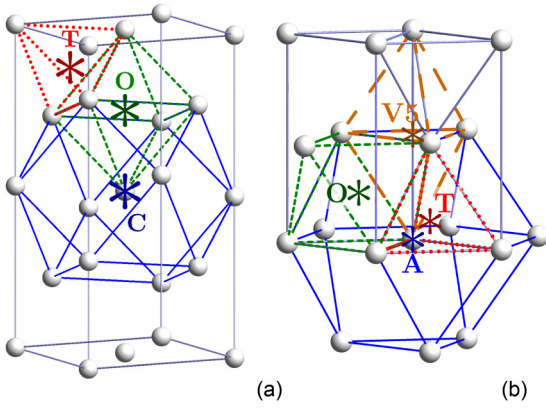


FIG. 1. Origins of the reference RDFs for fcc (a) and hcp (b) lattices. The origins marked by T (tetrahedral voids, red), O (octahedral voids, green), V5 (bipyramidal void, orange), and C or A (lattice nodes, blue) are shown with first coordination polyhedra shown with dotted, dashed, long-dashed, and solid lines, respectively.

Exceptions were detected for cramped structures of very tight or spacious sites. These structures, however, lie at very high energies, so large errors do not affect the results for the ground sites discussed here.

The parametric (ρ, ϵ) plane for the guest-host interaction was discretized as $0.25 \times 1.1^n \text{ cm}^{-1}$, $n = 0, \dots, 87$ for ϵ and $(0.3 + 0.1m) \text{ \AA}$, $m = 0, \dots, 97$ for ρ . N values were scanned from 0 to 24.

D. Structure analysis

By construction, N , the number of guest atoms removed, is uniquely defined by the convex hull analysis, and it confirms the effective size of a trapping site. However, it does not contain any information on the symmetry and structure of the corresponding site. It may well happen that distinct structures correspond to the same N , e.g., tetrahedral and octahedral interstitials in the fcc lattice [45,46].

Analysis of the radial distribution functions (RDFs) provides a computationally efficient and straightforward way to establish the origin of the stable trapping sites. (More elaborated techniques, like clustering, were shown to be excessive for the analysis of atomic guests [46].) Following Refs. [45,46], we introduced a set of reference RDFs for ideal lattices,

$$\tilde{q}_P(r) = \frac{1}{\sqrt{32\pi}\sigma} \sum_i \exp[-(r - r_{Pi})^2/2\sigma^2], \quad (4)$$

which is used in the form $q_P(r) = w(r)\tilde{q}_P(r)$ with $w(r) = 1/[4\pi \max(r_0, r)^2]$ and $r_0 = a/2$. Here $r_{Pi} = |\mathbf{x}_P - \mathbf{x}_i|$ gives the position of the host atom i with respect to some reference lattice point P . The choice of such origins for the fcc lattice is trivial [45,56]: it includes the centers of tetrahedral and octahedral voids and the lattice node, which has a cuboctahedral environment [T, O, and C points in Fig. 1(a), respectively]. For the hcp structure, the same choice looks natural [with a slight difference in the anticuboctahedral (A) environment of the node]. Also, the spacious bipyramidal void of the D_{3h}

TABLE I. Parameters of the LJ interactions used for RG crystals and optimized lattice constants and atomization energies per atom. Distances in angstroms, energies in wave numbers.

RG	ρ_{HH}	ϵ_{HH}	fcc		hcp	
			a	E^{at}	a	E^{at}
Ne	3.091	29	4.246	252.84	4.246	252.85
Ar	3.758	100	5.162	861.03	5.162	861.06
Kr	4.030	140	5.535	1205.44	5.535	1205.48
Xe	4.361	197	5.990	1696.23	5.990	1696.28

symmetry, hereafter V5, was added to this reference set; see Fig. 1(b).

For each stable accommodation, the RDF $q(r)$ is presented in the form of Eq. (4) but referenced to the guest atom (r_i replaces r_{Pi}). A comparison of the real RDFs computed across the (ρ, ϵ) domain, where the sites with given N are stable, with the reference RDFs suggests the type of guest lattice position. A more automatic auxiliary procedure involved the linear regression

$$\min \left\| q(r) - \sum_P W_P q_P(r) \right\|. \quad (5)$$

If the reference points are reasonably chosen, the regression coefficients W_P suggest the tentative guest position with respect to the lattice and the symmetry of its closest environment for any ρ, ϵ, N . When perfect matching with one of the reference positions occurs, $W_P = \delta_{PP'}$ for the sites of P' origin, so the deviation of the leading coefficient from unity reflects the uncertainty of assignment. The use of reference RDFs greatly reduces the need for visual inspections of the structures found.

III. RESULTS

A. Ideal fcc and hcp crystals

The LJ parameters for the host-host interactions are taken as the equilibrium properties of the potentials by Aziz and co-workers [55,57–59]. The advantage of the latter is that they provide realistic approximations to the two-body components of the more elaborate many-body *ab initio* potentials [25,48]. These parameters are listed in Table I together with the optimized lattice constants and atomization energy values. In agreement with the previous experience, the LJ model gives very similar lattice constants for two phases (note that for hcp we use $a_{\text{hcp}} = a/\sqrt{2}$) and a slight preference to the hcp lattice [20–23].

B. Mapping of N_0 : Sizes of the stable sites

At each point of the parameter plane (ρ, ϵ) , the convex hull analysis identifies all stable sites including the ground one having a certain effective size N_0 as is shown in Fig. 2 [examples of the $\Delta E(N)$ dependences at certain parameters are given below in Sec. IV]. Due to universal parameter scaling, the maps for each lattice type are similar for all hosts and likely exhaust all the generic ground stable sites for the LJ potential model.

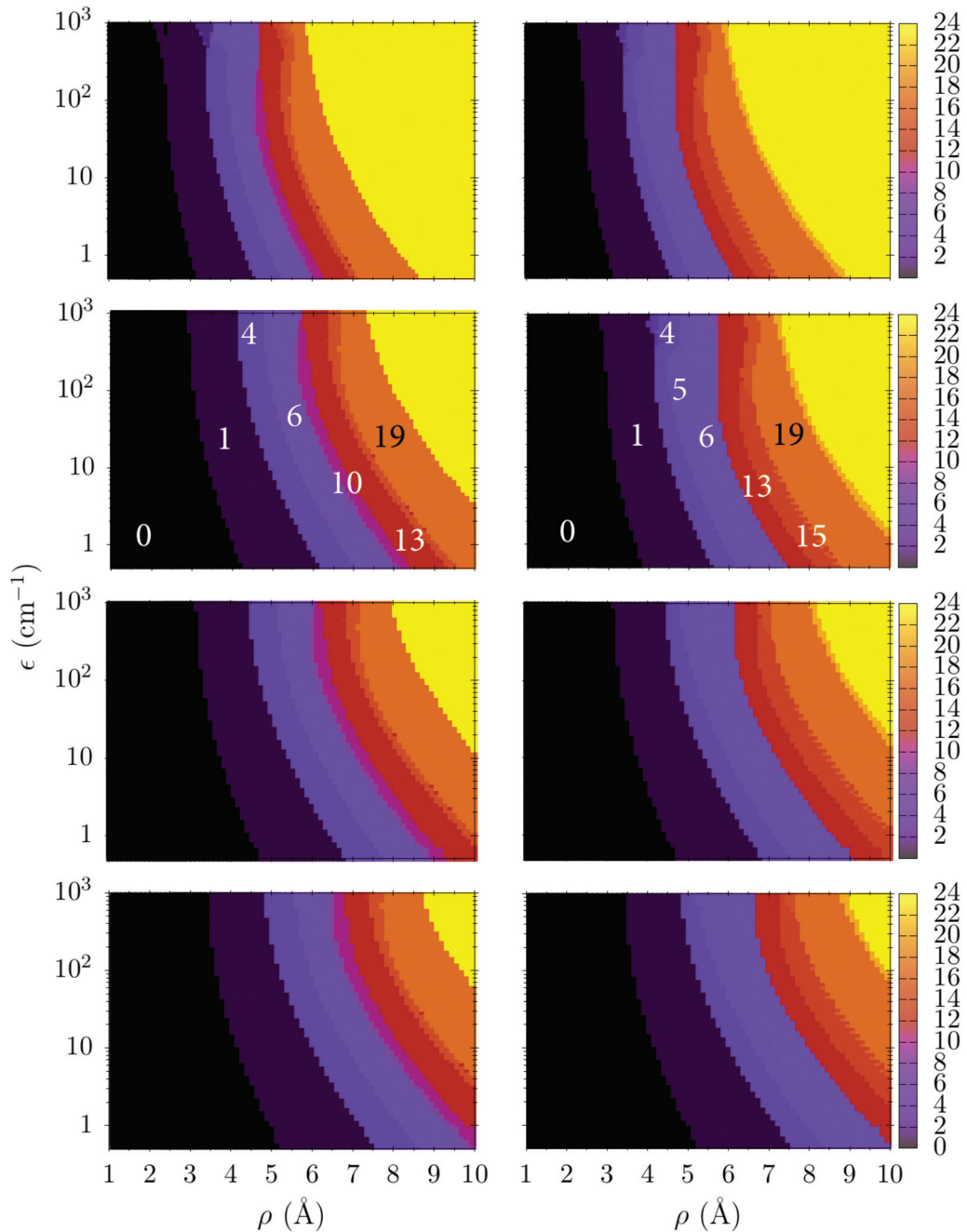


FIG. 2. Maps of the N_0 parameters for the ground sites in the LJ parameter space (ρ , ϵ). The rows from the top to the bottom present the results for Ne, Ar, Kr, and Xe; left and right columns correspond the fcc and hcp lattices, respectively. The bars on the right specify the N_0 color coding.

The results for the fcc lattice essentially confirm the findings of Refs. [45,46] for the case of the Ar host, namely that the accommodations with $N_0 = 0, 1, 4$, and 6 are stable. Extension of the ρ range and use of the finer parameter space scanning bring five new stable sites with $N_0 = 8, 10, 13, 16$, and 19 . The domains where most of these sites correspond to the ground accommodation are marked in Fig. 2 for Ar ($N_0 = 8$ and 16 domains form very tiny strips between those of $N_0 = 6, 10$ and $N_0 = 13, 19$, respectively). Regular patterns can also be found among the larger structures, e.g., $N_0 = 20, 28, 29, \dots$, but we did not analyze them here as they

appear at nonphysical interaction parameters. The structures with $N_0 > 13$ may also not be realistic except for the Ne host. The case of the hcp lattice reveals stable structures with $N_0 = 0, 1, 4, 5, 6, 13, 15$, and 19 . For both lattices, N_0 strongly correlates with the interaction range ρ ($N_0 \sim \rho^{2+\alpha}$, $\alpha \leq 1$) and exhibits a weaker dependence on interaction energy ϵ .

Comparing accommodations in the fcc and hcp lattices, we consider the difference between the ground accommodation energies,

$$\Delta E_{\text{fcc/hcp}} = \Delta E_{\text{fcc}}(N_0^{\text{fcc}}) - \Delta E_{\text{hcp}}(N_0^{\text{hcp}}),$$

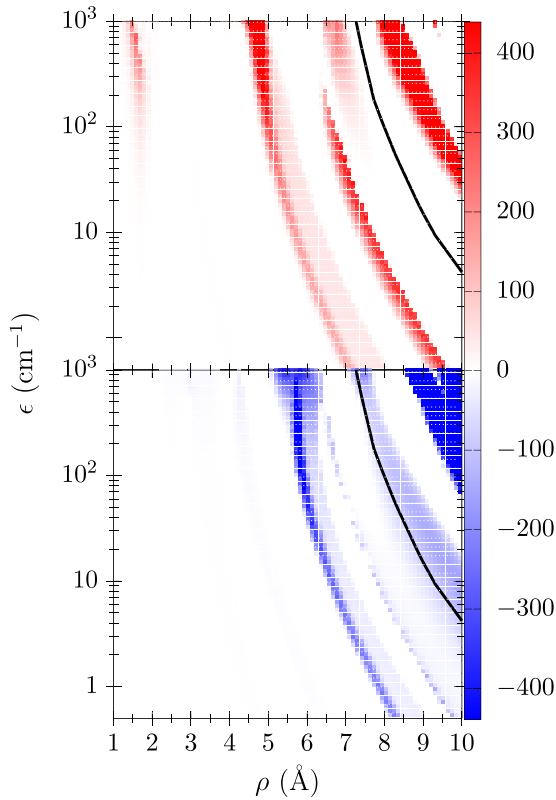


FIG. 3. The maps of $\Delta E_{\text{fcc/hcp}}$, accommodation energy difference between fcc and hcp phases, for Ar hosts. Top and bottom panels show the regions of preferable accommodation in the hcp and fcc phases, respectively. Black lines delineate top-right corners populated by the sites with $N_0 > 19$ not analyzed here.

at each (ρ, ϵ) point. This difference indicates which phase would preferably accommodate a certain guest atom disregarding the phase coexistence, the trapping mechanism, and the local phase transition. Note that for each phase accommodation energy (2) is referred to distinct energy limits, which cannot be connected to each other within the LJ model wrongly favoring the hcp phase. Nevertheless, it is still possible to make plausible predictions about the coarse energy scale. Indeed, assuming that the majority of the bulk contributions to the $E_{[\text{G}@\text{H}]}(N)$ terms of Eq. (2) cancel each other, and disregarding local lattice relaxation effects, $\Delta E_{\text{fcc/hcp}}$ can be estimated as $N_0^{\text{fcc}} E_{\text{fcc}}^{\text{at}} - N_0^{\text{hcp}} E_{\text{hcp}}^{\text{at}}$. In the case of equivalent effective trapping site sizes, $N_0^{\text{fcc}} = N_0^{\text{hcp}} = N_0$, the energy difference $\Delta E_{\text{fcc/hcp}} \approx N_0(E_{\text{fcc}}^{\text{at}} - E_{\text{hcp}}^{\text{at}})$ is directly affected by the wrong phase stability and other minor effects. In the opposite case, $\Delta E_{\text{fcc/hcp}} \approx (N_0^{\text{fcc}} - N_0^{\text{hcp}})E_{\text{fcc}}^{\text{at}}$. Taking the maximum N considered here, i.e., 24, and the maximum difference in fcc and hcp atomization energies for Xe, 0.05 cm^{-1} (see Table I), we can estimate the uncertainty of the phase preference prediction in our model as a few wave numbers. The same uncertainty estimate (with correct opposite sign) can be derived from the accurate atomization energy values computed for Ar in Ref. [27]. It is much lower than the E^{at} values themselves.

The maps of $\Delta E_{\text{fcc/hcp}}$ for Ar are shown in Fig. 3, where the top and bottom panels correspond to the regions of the preferred hcp and fcc accommodations, respectively.

Accommodation energies are the same for the two phases in the most important part of the entire parameter plane, where the guest-host interaction is weaker than the host-host one. This indicates that the structures of the trapping sites in both lattices are very close to each other. However, as the guest-host interaction range and, consequently, N_0 increase, the narrow strips with alternating fcc-hcp preference emerge. As expected, the origin is the difference in the effective volumes occupied by the guest in two phases; cf. Figs. 2 and 3. First, the stable hcp $N_0 = 5$ site emerges being stabilized with respect to the $N_0 = 6$ site in the fcc lattice. Then, the fcc $N_0 = 8$ and 10 accommodations become more stable than the hcp $N_0 = 13$ alternative. As ρ grows further, the $N_0 = 15$ hcp site gains preference over the $N_0 = 16$ accommodation in the fcc lattice. The alterations continue for the sites $N_0 > 19$, delineated in Fig. 3 by black lines, but we did not analyze them as they are probably not feasible for atomic impurities.

The maps show that atomic impurity, depending on the range and strength of its interaction with the host atoms, may have a clear preference for the fcc or hcp accommodation. This preference is mainly determined by the effective size of the trapping site, with tighter sites always favored. In the case of Ar, $|\Delta E_{\text{fcc/hcp}}|$ approaches $\sim 400 \text{ cm}^{-1}$. That means that a single impurity may be worth more than 1000 differences in atomization energies between the fcc and hcp lattices [27].

C. RDF analysis

Figure 4 illustrates the radial distribution functions obtained for the ground stable sites in the Ar hcp lattice. A comparison with the reference RDFs classifies $N_0 = 1, 13,$ and 15 sites as being anticuboctahedral and $N_0 = 4$ as tetrahedral. The coexistence of several types can be suggested for the $N_0 = 0$ and 19 cases. The bipyramidal V5 type is represented by $N_0 = 0$ and 5 sites. An example of a similar comparison for small fcc sites can be found in Ref. [45]. In combination with the present results, it establishes $N_0 = 0, 4,$ and 16 sites as tetrahedral, another $N_0 = 0$ and $N_0 = 6, 8, 10$ as octahedral, and $N_0 = 1, 13, 19$ as cuboctahedral.

The RDF analysis makes it possible to classify the site types over the entire parameter plane, as is shown in Fig. 5 for both fcc and hcp lattices of Ar. Regression (5) was used first to color the points where the dominant weight W_p exceeded 0.9. Otherwise, the long-range part of the RDFs was inspected visually to find the best correspondence with one of the references. Note that $N_0 = 0$ sites appearing at very small ρ , comparable to host van der Waals radius $\rho_{\text{HH}}/2 \approx 2 \text{ \AA}$, should be discarded from the analysis.

D. Structure overview

Presenting the structures of the generic sites, it is convenient to follow their symmetry types and consider two lattices in parallel. Schematic illustrations are drawn, for clarity, for ideal unperturbed lattices. Their local symmetry confirmed through the symmetry of the first coordination polyhedron, however, is the same as that in the optimized structures.

The smallest interstitial $N_0 = 0$ sites in both lattices are tetrahedral. Their structures shown in Figs. 6(a) and 6(b) for fcc and hcp crystals, respectively, correspond to impurity

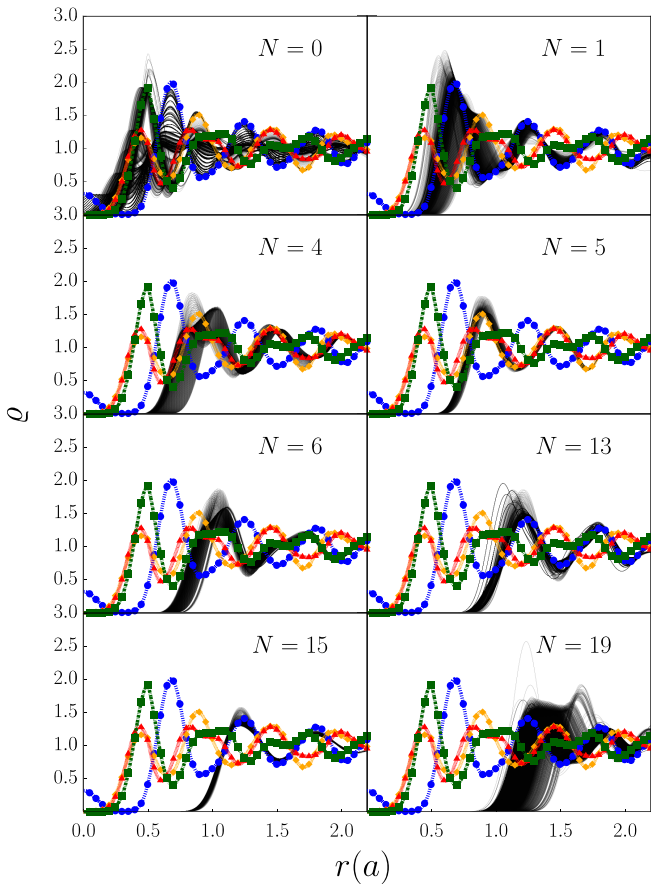


FIG. 4. Radial distribution functions for the ground stable sites in the Ar hcp lattice shown as the thin black lines. Lines with symbols correspond to the reference RDFs: red triangles for tetrahedral, blue dots for anticuboctahedral, green squares for octahedral, and orange diamonds for bipyramidal reference points, respectively (see Fig. 1 for definition). Note that distances are given in units of the lattice parameter a .

placed in the tetrahedral lattice voids, and they have identical coordination polyhedra of perfect T_d symmetry. The next stable tetrahedral site in both lattices, $N_0 = 4$, is derived from these interstitials by removing four host atoms forming the closest tetrahedron. In the fcc $N_0 = 4$ site, the guest atom is coordinated by the frustum of the tetrahedron with T_d symmetry [see Fig. 6(c)], while the symmetry of its hcp counterpart is reduced to axial C_{3v} [Fig. 6(d)]. In the fcc lattice, removal of the next coordination polyhedron consisting of 12 host atoms gives the stable $N_0 = 16$ site that maintains T_d symmetry. No other tetrahedral ground sites emerge in the hcp lattice below $N_0 = 20$.

Placement of impurity into octahedral voids produces the second type of interstitials $N_0 = 0$ in both lattices. Figures 7(a) and 7(b) show the structures of the perfect O_h local symmetry. Upon removing the six-atom coordination octahedron, one arrives at the $N_0 = 6$ stable sites, which are generic for both lattices [Figs. 7(c) and 7(d)]. The fcc lattice maintains an O_h environment, while in hcp the symmetry lowers to D_{3d} . This exhausts the generic octahedral type in hcp with $N_0 < 20$, whereas two more sites of this type, $N_0 = 8$ and 10, were found in the fcc lattice. Both can be derived from

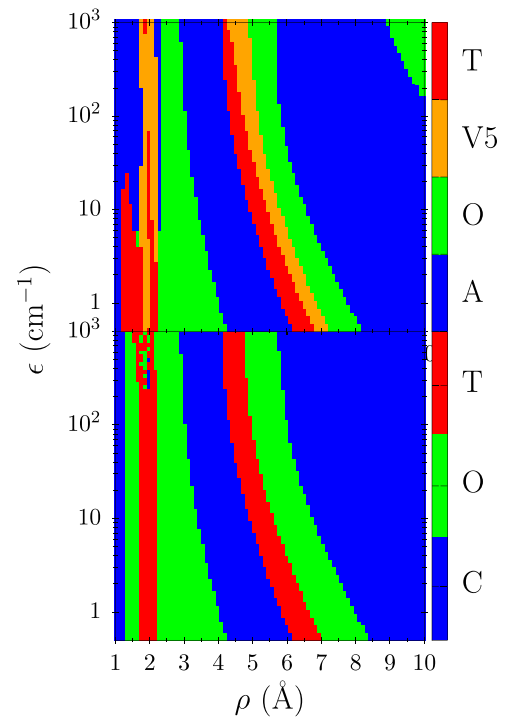


FIG. 5. Maps of the structural types of the ground sites in the LJ parameter plane (ρ , ϵ) according to the RDF analysis. The top and bottom panels present the hcp and fcc Ar lattices, respectively. The bars on the right specify the color coding according to the reference RDF types, tetrahedral (T), octahedral (O), and cuboctahedral (C) for fcc lattice, and tetrahedral (T), octahedral (O), anticuboctahedral (A), and bipyramidal (V5) for hcp lattice. See Sec. IID for explanations.

$N_0 = 6$ by removing two host atoms lying on the edge of the coordination cube or four host atoms lying on its face, respectively. Their symmetries are C_{2v} and C_{4v} .

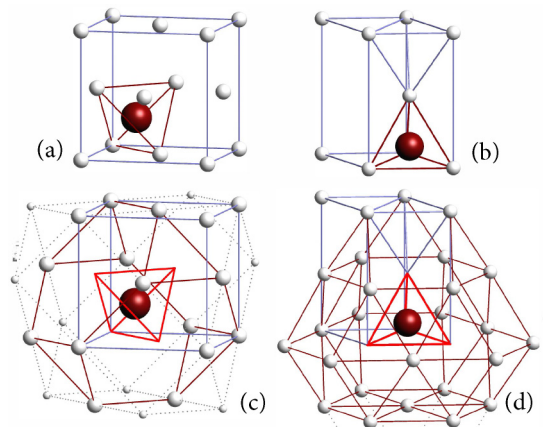


FIG. 6. Schematic structures of the tetrahedral stable sites derived from the ideal lattices. (a),(b) $N_0 = 0$ interstitials in fcc and hcp lattices; (c),(d) $N_0 = 4$ sites in fcc and hcp lattices. Guest atom is represented by a large sphere; host atoms forming an initial cell and a first coordination shell are shown as medium spheres connected by colored solid lines. Small spheres indicate other host atoms added for presentation clarity.

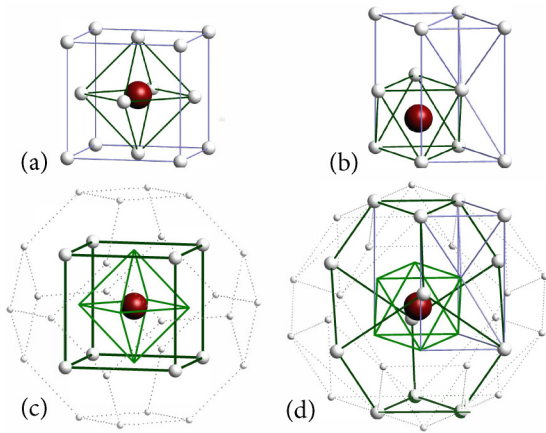


FIG. 7. Same as Fig. 6, but the octahedral stable sites. (a),(b) $N_0 = 0$ interstitials in fcc and hcp lattices; (c),(d) $N_0 = 6$ sites in fcc and hcp lattices.

A single substitution produces the stable $N_0 = 1$ sites coordinated by the perfect O_h cuboctahedron in fcc and anticuboctahedron (hexagonal cuboctahedron) of D_{3h} symmetry in hcp; see Figs. 8(a) and 8(b). Then the $N_0 = 13$ sites follow with the missed first coordination polyhedra at the substituted node [Figs. 8(c) and 8(d)]. They maintain the local symmetries of the precursors. Upon removing the next six neighbors, one arrives at the $N_0 = 19$ sites, which are stable in both fcc and hcp lattices, again of O_h and D_{3h} coordination. Lattice relaxation of these spacious sites renders a very strong dependence of their geometry on guest-host interaction parameters, which, in turn, blurs the RDF distributions shown in Fig. 4. Study of the hexagonal packing reveals one more stable site not present in the fcc case, i.e., the $N_0 = 15$ site. It can be viewed as an $N_0 = 13$ structure without two more nearest-neighbor host atoms. In contrast to the fcc $N_0 = 8, 10$ cases discussed above, we detected a set of structures that differ by missing pairs with the highest symmetry C_{2v} .

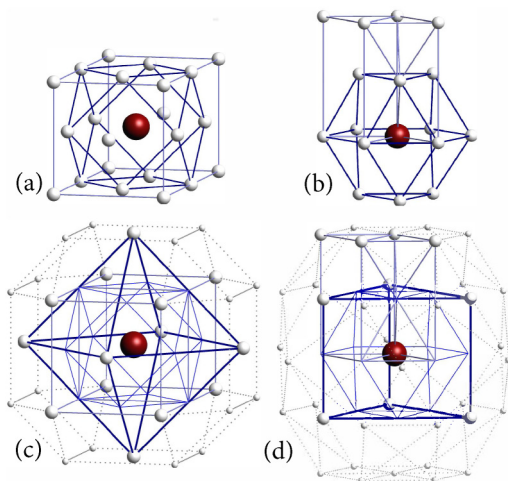


FIG. 8. Same as Fig. 6, but the cuboctahedral/anticuboctahedral stable sites. (a),(b) $N_0 = 1$ interstitials in fcc and hcp lattices; (c),(d) $N_0 = 13$ sites in fcc and hcp lattices.

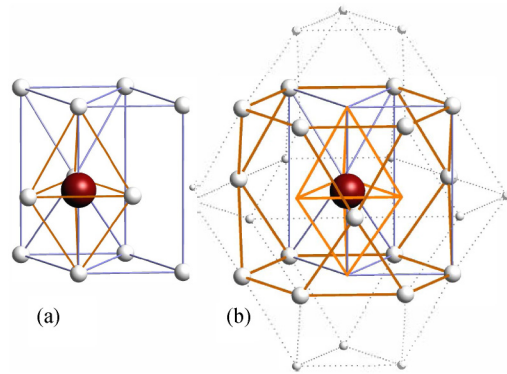


FIG. 9. Same as Fig. 6, but the bipyramidal stable sites in an hcp lattice. (a) $N_0 = 1$ interstitial, (b) $N_0 = 5$ site.

Bipyramidal (V5) structures are typical only to an hcp lattice. Two stable sites, namely the third interstitial $N_0 = 0$ and $N_0 = 5$, are shown in Fig. 9. In both sites, the impurity has a D_{3h} local environment.

IV. DISCUSSION

Extensive computational analysis of the LJ model of an atom embedded in the fcc and hcp rare-gas solids revealed a handful of the thermodynamically stable trapping sites that can provide the lowest-energy guest accommodation. They are classified by the number of host atoms substituted by a guest, or the effective size, and by structure type, or the location of the guest close to a certain lattice point. For physically relevant ranges of the guest-host interaction parameters, the fcc list is $N_0 = 0(\text{T}), N_0 = 0(\text{O}), N_0 = 1(\text{C}), N_0 = 4(\text{T}), N_0 = 6(\text{O}), N_0 = 8(\text{O}), N_0 = 10(\text{O}), N_0 = 13(\text{C}), N_0 = 16(\text{T}),$ and $N_0 = 19(\text{C})$, where T, O, and C relate the site type to the tetrahedral void, the octahedral void, and the node of the fcc cell. In the hcp lattice, the stable site set includes $N_0 = 0(\text{T}), N_0 = 0(\text{V5}), N_0 = 0(\text{O}), N_0 = 1(\text{A}), N_0 = 4(\text{T}), N_0 = 5(\text{V5}), N_0 = 6(\text{O}), N_0 = 13(\text{A}), N_0 = 15(\text{A}),$ and $N_0 = 19(\text{A})$, where A corresponds to the node replacing C in the fcc cell, and V5 is associated with the bipyramidal void; see Fig. 1.

In principle, the mapping of the ground sites and their types onto the guest-host parameter plane allows one to predict the most probable accommodation of any S-state atom provided that its interaction parameters with the host atom are known. We had shown elsewhere [45] that such predictions on the ground site structure and the number of stable sites indeed agree with more sophisticated simulations and well-interpreted experimental absorption, excitation, and ESR spectroscopy data for H, Mn, Na, Ba, Eu, and Yb atoms isolated in an Ar matrix.

Enlisted ground accommodations tightly pave the entire parameter plane and thus they are generic. However, the question arises as to whether or not new unlisted site types can be found with finer discretization of the continuous parameter space. One argument against this possibility can be found in the analysis of the sites, which, according to the convex hull concept, are stable but lie above the ground in energy. Applying precisely the same symmetry and structure analysis as exposed for the ground sites, we found that in both lattices

practically all $N \neq N_0$ stable sites belong to the above lists. One exception is known for the fcc lattice: the $N = 7(O)$ site [39,45] of C_{3v} symmetry that is derived from $N_0 = 6$ by removing one host atom from its coordination cube; see Fig. 7(c). Two rare exceptions of the anticuboctahedral type were found in the hcp lattice at $N = 2$ and 3. The corresponding structures have C_{2v} and C_{3v} symmetries. The sporadic appearance of some $N \geq 14$ structures was also detected, but at very high energy. It is unlikely that any other accommodation can appear as the ground one to append generic sites already enlisted. Of course, these findings are valid only for the LJ model, and nothing prevents the formation of other ground sites in the models with more elaborate realistic potentials. Such deviations from LJ motifs would indicate qualitatively important effects in the guest-host interactions.

Our classification of the generic sites by type uncovers quite a simple rule: the majority of the sites can be derived from interstitials and single substitution by sequential removal of their coordination polyhedra. Exceptions are fcc $N_0 = 8, 10$ and hcp $N_0 = 15$, which can be viewed as the partial polyhedron destruction. An important difference between the two lattices is that the fcc sites that follow the rule maintain high polyhedral symmetry, T_d or O_h , while coordination of the hcp sites generally has lower symmetry. Indeed, only two interstitial hcp sites possess perfect T_d and O_h coordinations. All others have only one threefold symmetry axes. It has an interesting implication to optical spectroscopy of the matrix-isolated S-state atoms. Bright states normally have P-symmetry associated with a unit electron orbital (or total) angular momentum. Triple degeneracy in momentum projection remains in polyhedral environments with groups having an irreducible representation of dimension 3, it splits to 2+1 for axial groups with the axis order 3 or higher, and it is fully lifted for lower symmetries. A more realistic picture of the dynamic Jahn-Teller effect [60] tells us that in the former case, the single absorption band should appear with a triplet structure, while in the second case two bands would emerge, one with a secondary doublet structure. Three separate bands are expected in the latter case. To our knowledge, the only firm experimental observation of the 2+1 bands through fluorescence excitation spectroscopy was reported for Ba by McCaffrey and co-workers [37,38]. They were interpreted as belonging to the axially symmetric $N = 7$ fcc site mentioned above [39] and/or to a stacking fault accommodation, very similar to the hcp $N_0 = 5$ site reported here [37]. It is true that such assignments require extensive and sophisticated modeling and meet uncertainty due to the overlapping of broad bands, but the understanding that the hcp phase should likely give more complex band shapes than the fcc phase may be taken as a useful hint.

Accommodations in two lattices can be compared not only in symmetry but also in energy. Despite the wrong preference of the hcp phase inherent to the LJ model, it is still possible to discern the situations when accommodation in one of the phases is strongly preferred. Our analysis showed that they emerge when the effective sizes of the ground sites N_0 in two phases differ from one another; see Fig. 3. The structures of small fcc and hcp sites up to $N_0 = 6$ are very similar, so the only case of a sharp hcp preference is related to the bipyramidal $N_0 = 5$ accommodation, which is more

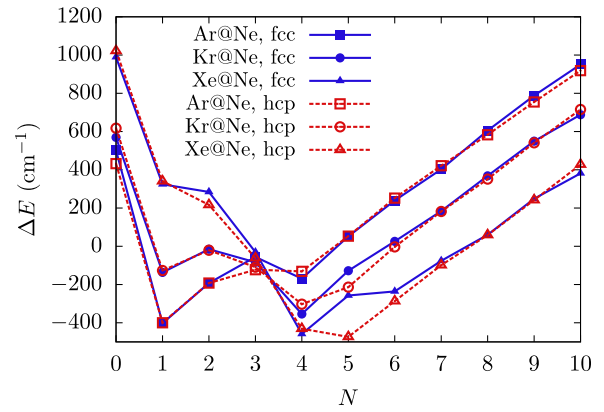


FIG. 10. The $\Delta E(N)$ dependence for Ar, Kr, and Xe guests in the Ne crystals.

stable with respect to the fcc $N_0 = 6$ accommodation. For the guest-host interactions of longer range, fcc accommodation appears to be preferred due to axially symmetric $N_0 = 8, 10$ sites that coexist with $N_0 = 13$ in hcp phase. Then hcp is preferred again because the $N_0 = 15$ site gains energy with respect to the fcc $N_0 = 16$. These qualitative considerations are valid only within the LJ model, and they have nothing to do with the intricate issue of phase transitions in the presence of impurities. They can only suggest that for some atomic impurities, an hcp environment should be considered as quite realistic.

To illustrate the use of these results, we consider the stable sites of Ar, Kr, and Xe atoms in Ne crystals in relation to Ref. [43], which indicated the preference of the hcp accommodations. For compatibility with the RG-RG LJ potentials, the ρ and ϵ LJ parameters for Ne-RG pairs were taken from Refs. [61,62]. The $\Delta E(N)$ diagrams with these parameters for both the fcc and hcp phases are shown in Fig. 10. According to the convex hull concept, stable fcc sites include $N = 0, 1, 4, 6$, plus marginal stability can also be guessed for $N = 7$ and 8. In the hcp lattice, $N = 0, 1, 4$, and 5 sites appear as stable. All of them are identified by the global optimization and described above. In the fcc phase, Ar tends to substitute one Ne atom, while its accommodation in the $N = 4$ tetravacancy is less probable. The order of these sites in energy is changed for Kr and Xe. In the latter case, the $N = 6$ hexavacancy becomes a more preferable secondary accommodation than the $N = 1$ one. This pattern illustrates the smooth changes in the lowest energy sites as the effective size of the guest increases (along the Ar, Kr, Xe sequence, ρ goes from 3.14 to 3.86 Å, while ϵ is about 50 cm⁻¹ and does not change much [61,62]). Ar and Kr accommodations in the hcp lattice follow a very similar trend. The slight preference of the fcc phase at $N = 4, 6$ originating from different lattice relaxation energy may not be considered as significant due to the simplicity of the potential model and the omission of entropy contributions. A qualitative difference should be noted only in the case of Xe, where the ground sites in the two lattices are distinct: $N_0 = 4$ fcc and $N_0 = 5$ hcp. Although their energy mismatch is still beyond the expected accuracy of the model, one can suggest that such a qualitative difference may give

strong preference to accommodation in one of the phases and even cause local rearrangement of the host structure.

V. CONCLUSIONS

A comprehensive computational analysis of the stable trapping sites of an atomic guest in the LJ fcc and hcp rare-gas lattices reveals a limited number of generic structures that may appear to be the lowest energy accommodation. Most of the structures found can be derived from the interstitial and substitutional accommodations by successive removal of the first coordination polyhedra. Generally, those typical of the fcc lattice possess higher polyhedral symmetry in comparison to hcp structures with predominantly axial symmetries. The cases of a strong preference of guest accommodation in one phase or another are identified and discussed. They take

place when one phase offers a tighter guest accommodation than the other. The corresponding difference between the accommodation energy is much larger than the overall phase stability difference, and thus it can be discerned even within the LJ model, which notoriously favors the hcp phase. The implications of the present generic results to matrix isolation spectroscopy are briefly discussed and illustrated for Ar, Kr, and Xe atoms trapped in Ne crystals.

The data that support the findings of this study are available from the corresponding author upon reasonable request.

ACKNOWLEDGMENT

Financial support by the Russian Science Foundation under Project No. 17-13-01466 is gratefully acknowledged.

All authors contributed equally to this work.

-
- [1] E. Whittle, D. A. Dows, and G. C. Pimentel, *J. Chem. Phys.* **22**, 1943 (1954).
- [2] S. Cradock and A. Hinchcliffe, *Matrix Isolation: A Technique for the Study of Reactive Inorganic Species* (Cambridge University Press, Cambridge, 1975).
- [3] M. J. Almond, R. J. H. Clark, and A. J. Downs, *Spectroscopy of Matrix Isolated Species*, edited by R. J. H. Clark and R. E. Hester (Wiley, New York, 1989), Vol. 17.
- [4] I. R. Dunkin, *Matrix-isolation Techniques: A Practical Approach* (Oxford University Press, Oxford, 1998).
- [5] M. E. Jacox, *Acc. Chem. Res.* **37**, 727 (2004).
- [6] Y. A. Dmitriev, *Low Temp. Phys.* **33**, 493 (2007).
- [7] V. I. Feldman, F. F. Sukhov, and A. Y. Orlov, *J. Chem. Phys.* **128**, 214511 (2008).
- [8] L. H. Jones, S. A. Ekberg, and B. I. Swanson, *J. Chem. Phys.* **85**, 3203 (1986).
- [9] M. A. Collier, O. Byrne, C. Murray, and J. G. McCaffrey, *J. Chem. Phys.* **132**, 164512 (2010).
- [10] A. V. Danilychev and V. A. Apkarian, *J. Chem. Phys.* **99**, 8617 (1993).
- [11] M. Prager and W. Langel, *J. Chem. Phys.* **88**, 7995 (1988).
- [12] M. Prager and A. Heidemann, *Chem. Rev.* **97**, 2933 (1997).
- [13] P. Roubin, S. Varin, C. Crépin, B. Gauthier-Roy, A.-M. Flank, P. Lagarde, and F. Ténégal, *Low Temp. Phys.* **26**, 691 (2000).
- [14] N. A. Young, *Coord. Chem. Rev.* **277-278**, 224 (2014).
- [15] M. L. Klein and J. A. Venables, *Rare Gas Solids* (Academic, London, 1976), Vol. 1.
- [16] C. S. Barrett and L. Meyer, *J. Chem. Phys.* **41**, 1078 (1964).
- [17] L. Meyer, C. S. Barrett, and P. Haasen, *J. Chem. Phys.* **40**, 2744 (1964).
- [18] Y. Sonnenblick, E. Alexander, Z. Kalman, and I. Steinberger, *Chem. Phys. Lett.* **52**, 276 (1977).
- [19] Y. Sonnenblick, Z. Kalman, and I. Steinberger, *J. Cryst. Growth* **58**, 143 (1982).
- [20] T. Kihara and S. Koba, *J. Phys. Soc. Jpn.* **7**, 348 (1952).
- [21] T. H. K. Barron and C. Domb, *Proc. R. Soc. London, Ser. A* **227**, 447 (1955).
- [22] B. W. van de Waal, *Phys. Rev. Lett.* **67**, 3263 (1991).
- [23] P. Schwerdtfeger, N. Gaston, R. P. Krawczyk, R. Tonner, and G. E. Moyano, *Phys. Rev. B* **73**, 064112 (2006).
- [24] B. Borden and C. Radin, *J. Chem. Phys.* **75**, 2012 (1981).
- [25] K. Rościszewski, B. Paulus, P. Fulde, and H. Stoll, *Phys. Rev. B* **62**, 5482 (2000).
- [26] B. W. van de Waal, *J. Cryst. Growth* **309**, 181 (2007).
- [27] P. Schwerdtfeger, R. Tonner, G. E. Moyano, and E. Pahl, *Angew. Chem. Int. Ed.* **55**, 12200 (2016).
- [28] J. K. Dewhurst, R. Ahuja, S. Li, and B. Johansson, *Phys. Rev. Lett.* **88**, 075504 (2002).
- [29] N. V. Krainyukova, R. E. Boltnev, E. P. Bernard, V. V. Khmelenko, D. M. Lee, and V. Kiryukhin, *Phys. Rev. Lett.* **109**, 245505 (2012).
- [30] B. Li, G. Qian, A. R. Oganov, S. E. Boulfelfel, and R. Faller, *J. Chem. Phys.* **146**, 214502 (2017).
- [31] A. D. Rosa, G. Garbarino, R. Briggs, V. Svitlyk, G. Morard, M. A. Bouhfid, J. Jacobs, T. Irifune, O. Mathon, and S. Pascarelli, *Phys. Rev. B* **97**, 094115 (2018).
- [32] L. H. Jones and S. A. Ekberg, *J. Chem. Phys.* **87**, 4368 (1987).
- [33] W. Langel, W. Schuller, E. Knözinger, H.-W. Flegler, and H. J. Lauter, *J. Chem. Phys.* **89**, 1741 (1988).
- [34] M. Prager and W. Langel, *J. Chem. Phys.* **90**, 5889 (1989).
- [35] M. Prager, B. Asmussen, and C. J. Carlile, *J. Chem. Phys.* **100**, 247 (1994).
- [36] Y. Dmitriev, V. Melnikov, K. Styrov, and N. Benetis, *Phys. B* **458**, 44 (2015).
- [37] B. M. Davis, B. Gervais, and J. G. McCaffrey, *J. Chem. Phys.* **148**, 124308 (2018).
- [38] B. Davis and J. G. McCaffrey, *J. Phys. Chem. A* **122**, 7339 (2018).
- [39] N. N. Kleshchina, I. S. Kalinina, I. V. Leibin, D. S. Bezrukov, and A. A. Buchachenko, *J. Chem. Phys.* **151**, 121104 (2019).
- [40] A. C. Becker, K.-P. Lodemann, and U. Schurath, *J. Chem. Phys.* **87**, 6266 (1987).
- [41] M. Chergui, N. Schwentner, and V. Chandrasekharan, *J. Chem. Phys.* **89**, 1277 (1988).
- [42] R. L. Redington, *J. Chem. Phys.* **102**, 7332 (1995).
- [43] I. Fugol, Y. Rybalko, and E. Savchenko, *Solid State Commun.* **60**, 495 (1986).

- [44] D. Horinek and B. Dick, *Z. Phys. Chem.* **214**(2000).
- [45] G. K. Ozerov, D. S. Bezrukov, and A. A. Buchachenko, *Low Temp. Phys.* **45**, 301 (2019).
- [46] G. K. Ozerov, D. S. Bezrukov, and A. A. Buchachenko, *Phys. Chem. Chem. Phys.* **21**, 16549 (2019).
- [47] L.-G. Tao, N. N. Kleshchina, R. Lambo, A. A. Buchachenko, X.-G. Zhou, D. S. Bezrukov, and S.-M. Hu, *J. Chem. Phys.* **143**, 174306 (2015).
- [48] N. N. Kleshchina, K. A. Korchagina, D. S. Bezrukov, and A. A. Buchachenko, *J. Phys. Chem. A* **121**, 2429 (2017).
- [49] Q. Zhu, L. Li, A. R. Oganov, and P. B. Allen, *Phys. Rev. B* **87**, 195317 (2013).
- [50] Q. Zhu, A. R. Oganov, and X.-F. Zhou, in *Topics in Current Chemistry* (Springer International Publishing, Berlin, 2014), pp. 223–256.
- [51] A. A. Frost, *J. Am. Chem. Soc.* **73**, 2680 (1951).
- [52] N. Metropolis, A. W. Rosenbluth, M. N. Rosenbluth, A. H. Teller, and E. Teller, *J. Chem. Phys.* **21**, 1087 (1953).
- [53] P. J. M. van Laarhoven and E. H. L. Aarts, *Simulated Annealing: Theory and Applications* (Springer, the Netherlands, 1987).
- [54] *Search Methodologies: Introductory Tutorials in Optimization and Decision Support Techniques*, 2nd ed., edited by E. K. Burke and G. Kendall (Springer, US, 2014).
- [55] R. A. Aziz, *J. Chem. Phys.* **99**, 4518 (1993).
- [56] C. Crepin-Gilbert and A. Tramer, *Int. Rev. Phys. Chem.* **18**, 485 (1999).
- [57] R. A. Aziz and M. Slaman, *Chem. Phys.* **130**, 187 (1989).
- [58] R. A. Aziz, A. K. Dham, A. Allnatt, and W. J. Meath, *Mol. Phys.* **67**, 1291 (1989).
- [59] A. K. Dham, W. J. Meath, A. Allnatt, R. A. Aziz, and M. Slaman, *Chem. Phys.* **142**, 173 (1990).
- [60] I. B. Bersuker, *The Jahn-Teller Effect* (Cambridge University Press, Cambridge, 2006).
- [61] R. A. Aziz and A. van Dalen, *J. Chem. Phys.* **81**, 779 (1984).
- [62] D. A. Barrow, M. J. Slaman, and R. A. Aziz, *J. Chem. Phys.* **91**, 6348 (1989).